ACS APPLIED MATERIALS & INTERFACES

Research Article

www.acsami.org

Synthesis of Ultrasmall Platinum Nanoparticles on Polymer Nanoshells for Size-Dependent Catalytic Oxidation Reactions

Licheng Bai,[†] Shumeng Zhang,[†] Qiang Chen,*[,‡] and Chuanbo Gao*[,†]

[†]Center for Materials Chemistry, Frontier Institute of Science and Technology, Xi'an Jiaotong University, Xi'an, Shaanxi 710054, China

[‡]School of Chemical Engineering and Technology, Xi'an Jiaotong University, Xi'an, Shaanxi 710049, China

Supporting Information

ABSTRACT: It is highly desirable for the synthesis and stabilization of noble metal nanoparticles of uniform, precisely tunable sizes, especially in the range of angstroms to a few nanometers, for many catalytic applications in pursuit of optimal activity and selectivity. Herein, we report a novel strategy for the synthesis of uniform platinum (Pt) nanoparticles of ultrasmall sizes (average size: 0.9−2.3 nm), which are stabilized on hollow polymer nanoshells formed by polymerization of sodium dodecyl benzenesulfonate (SDBS) at the interface of an ethanol/water emulsion. The resulting composite represents a highly active catalyst for effective oxidation of alcohols under ambient conditions. Strong size-dependent catalytic activity of Pt nanoparticles has been revealed in aerobic oxidation of 1-phenylethanol to yield acetophenone, demonstrating a volcano-shape profile, with Pt nanoparticles of ∼1.7 nm showing the highest activity. The size effect has been attributed to the size-dependent d-band electron structure of the Pt nanoparticles. This work reveals the size effect of Pt nanoparticles in general organic oxidation reactions, and thus provides a general methodology and a lot of opportunities in the design of metal-nanoparticle-based catalysts for fine-chemical production.

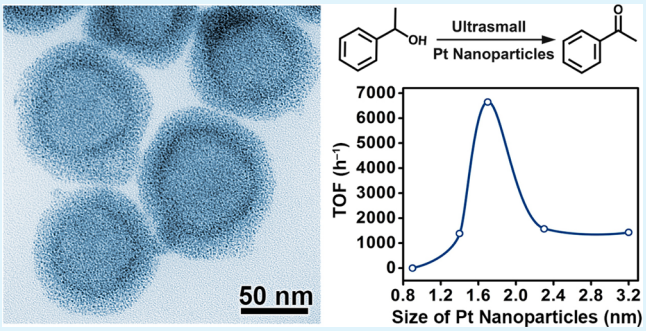

KEYWORDS: *ultrasmall noble metal nanoparticles, hollow nanospheres, stabilization, size control, size-dependent catalysis*

1. INTRODUCTION

Noble metal nanoparticles have opened up enormous opportunity in heterogeneous catalysis due to their excellent catalytic activity and selectivity in a variety of organic reactions, such as hydrogenation, oxidation, and coupling reactions.[1−3] Recent advances have demonstrated that the catalytic property of noble metal nanoparticles is highly dependent on their size,[4−16] morphology,[17−22] and composition.[23−25] However, a clear understanding of the relationship between the properties of the noble metal nanoparticles and their catalytic performance is still a grand challenge in the current research of metal catalysts for organic reactions, which, however, is critical to the advances of the design of the nanocatalysts. Among different properties, the size of noble metal nanoparticles represents one of the key factors that can impose a particularly strong effect on their catalytic property.[26] This effect dominates in Au-nanoparticle-catalyzed CO oxidation reactions, with nanoparticles of a specific, small size showing extremely high catalytic activity.[4,5] Similar effects can be observed in Pt-nanoparticle-catalyzed water−gas shift and electrochemical oxygen reduction reactions.[6−11] In addition to these gas-phase and electrochemical reactions, the maneuvering of the catalytic property by the nanoparticle size effect extents to many organic catalysis in recent years, although the explorations have been quite limited.[12−16,27−32] Prominently, the reaction selectivity was found to be greatly influenced by the nanoparticle size in a few Pt-nanoparticle catalyzed hydrogenation reactions.[27−32] In our previous work, we also observed strong effect of the particle size on the activity of a family of hydrogenation reactions.[33] This effect has been attributed to an increase in the exposed Pt atoms and surface unsaturated sites for nanoparticles of small sizes, and more importantly, to the modification of the d-band electron structure of the Pt nanoparticles that determines their interaction with the reactants and products. However, it is still unclear whether this size effect can be extendable to many other types of organic reactions, for example, oxidation reactions, which is another family of important reactions in chemical industry, thus becoming as a general rule in the design of metal-nanoparticle-based catalysts for a much broader scope of organic syntheses.

The maneuvering of the catalytic properties of metal nanoparticles requires that the nanoparticles can be synthesized with uniform, precisely tunable sizes, especially in the range of a few angstroms to nanometers, and that the nanoparticles can be stabilized on a support with high accessibility to suppress their

Received: January 2, 2017
Accepted: February 28, 2017
Published: February 28, 2017

DOI: 10.1021/acsami.6b16857
ACS Appl. Mater. Interfaces 2017, 9, 9710−9717

high tendency to aggregation. Typical strategies to stabilize these metal nanoparticles include microencapsulation in polymeric dendrimers,[7] inorganic metal oxide/carbon nanoshells,[34,35] and mesoporous materials.[36,37] However, it is still a grand challenge to achieve the stabilization effect together with high accessibility and precise size engineering of metal nanoparticles in a single system. Many investigations relied on catalysts with wide range of sizes, thus providing sample-averaged catalytic property of the metal nanoparticles, which led to ambiguity in designating the most active sizes of the nanoparticles accounting for the high catalytic property, unfavorable for pursuing optimal activity and selectivity.[38] Therefore, there is still a lot of room to develop alternative strategies in the design of supported metal-nanoparticle-based catalysts.

In this study, we start with a novel synthesis of polymer nanoshells by polymerizing sodium dodecyl benzenesulfonate (SDBS) at the interface of an ethanol/water emulsion, and develop a robust strategy to produce and stabilize Pt nanoparticles with uniform and precisely tunable sizes onto these shells for size-dependent catalysis. It is interesting that a solution of SDBS, a common anionic surfactant used in detergents, can form emulsions in a solvent of a certain polarity, which are able to polymerize with formaldehyde to afford robust polymer nanoshells. To the best of our knowledge, this hard-template-free synthesis of SDBS-formaldehyde polymer nanoshells was not reported in literature. The abundant sulfonate groups make the nanoshells highly dispersible, and capable of chemisorption of metal nanoparticles for their effective stabilization. By this means, uniform Pt nanoparticles of varying sizes (average size: 0.9−2.3 nm) have been produced and stabilized onto these polymer nanoshells in one pot. The nanoshell structure ensures that the Pt nanoparticles are highly accessible to reactants, without being significantly embedded within its interior space. With this composite, strong size effect of the Pt nanoparticles has been observed in aerobic oxidation of alcohols, with Pt nanoparticles of ∼1.7 nm showing the highest catalytic activity. The mechanism of the size-dependent catalysis has been further proposed and revealed with spectral evidence. We believe this study provides not only a general route to SDBS-formaldehyde polymer nanoshells as a novel support for metal nanoparticles, but also insights into the size effect of the nanocatalysts in a family of organic oxidation reactions for pursuing optimal catalytic properties.

2. EXPERIMENTAL SECTION

2.1. Materials. Sodium dodecyl benzenesulfonate (SDBS), formaldehyde (HCHO, 37 wt %), resorcinol, ammonium hydroxide ($NH_3 \cdot H_2O$, 28 wt %), potassium tetrachloroplatinate(II) (K_2PtCl_4, 99.9%), dimethyl sulfoxide (DMSO), 1-phenylethanol, 3,5,3′,5′-tetramethylbenzidine (TMB), carotene, mannite, catalase, superoxide dismutase (SOD), and ethanol (HPLC grade) were purchased from Sigma-Aldrich.

2.2. Synthesis of SF-Pt-*x* Hollow Nanospheres (*x* = 0.9, 1.4, 1.7, 2.3). In a typical synthesis of SF-Pt-1.7 hollow nanospheres, 0.3 g of SDBS was dissolved in a solution containing 125 mL of water, 50 mL of ethanol and 200 μL of $NH_3 \cdot H_2O$ (28 wt %) at 28 °C. To this solution was added 400 μL of HCHO (37 wt %) and 40 μL of K_2PtCl_4 (0.1 M) under vigorous stirring. After 36 h, the temperature was raised to 80 °C and maintained at this temperature for another 10 h, so that the polymerization degree of the SF polymer is increased for improved stability in catalytic oxidation reactions. The solid product was collected by centrifugation, washed with water/ethanol, and dried at 60 °C for 12 h. The size of the Pt nanoparticles can be conveniently tuned by adjusting the volume of the K_2PtCl_4 solution, with SF-Pt-0.9, -1.4, and -2.3 obtained by using 20, 30, and 60 μL of K_2PtCl_4 (0.1 M), respectively. The catalysts were denoted as SF-Pt-*x*, where *x* indicates the average size of the Pt nanoparticles in nanometer.

2.3. Catalytic Oxidation Reactions. In a typical catalytic oxidation reaction, 2 mL of the substrate (e.g., 1-phenylethanol) was mixed with the SF-Pt-*x* catalyst in a glass vial (20 mL capacity), with the headspace connected to the air via a needle. The reaction system was then stirred at a specific temperature (e.g., 80 °C). Aliquots of the products were withdrawn by a syringe at specific time intervals, which were then subjected to gas chromatography−mass spectrometry (GC−MS, Agilent 5975C with a thermal conductivity detector) analysis for calculating the conversion and selectivity of the reaction.

2.4. Oxygen Activation by the SF-Pt-*x* Catalysts. In a typical analysis, 20 μL of TMB (50 mM in ethanol) was dissolved in 2 mL of a HCOOH(0.2 M)/HCOONa (0.2 M) buffer solution. Then, 10 μL of an aqueous suspension of the SF-Pt-*x* catalyst was added into the solution. The concentrations of Pt in these solutions were 1 (Commercial Pt/C, ∼3.2 nm Pt), 0.72 (SF-Pt-2.3), 0.53 (SF-Pt-1.7), 0.44 (SF-Pt-1.4), and 0.31 $g \cdot L^{-1}$ (SF-Pt-0.9), respectively, so that the total quantity of exposed Pt atoms was kept the same for comparison. The UV−vis absorbance of the reaction solution at 652 nm was recorded at time intervals for evaluating the kinetics of the oxygen activation. In order to specify the species of the activated oxygen, different scavengers were added into the above solution prior to the UV−vis measurements: (1) Carotene (0.5 mg in DMSO); (2) Mannite (50 mM, 100 μL in water); (3) Catalase (4000 unit·mL^{-1}, 100 μL in water); and (4) SOD, (4000 unit·mL^{-1}, 100 μL in water). The UV−vis absorbance of the reaction system at 652 nm was then recorded after different lengths of time.

2.5. Characterization. High-resolution transmission electron microscopy (HRTEM) was performed on a Philips Tecnai F20 FEG-TEM with accelerating voltage of 200 kV. Scanning electron microscopy (SEM) and energy dispersive X-ray spectroscopy (EDS) were performed using a field-emission JSM-7000F microscope operated at an acceleration voltage of 15 kV. X-ray diffraction (XRD) patterns were recorded on a Rigaku SmartLab X-ray diffractometer equipped with Cu Kα radiation and D/teX Ultra detector, scanning from 20° to 80° (2θ) at the rate of 10° min^{-1}. UV−vis spectroscopy was performed on an Ocean Optics HR2000+ES UV−vis−NIR spectrophotometer with a DH-2000-Bal light source. Dynamic light scattering (DLS) was performed on a Beckman Coulter Delsa Nano C particle analyzer. Elemental analysis was conducted by inductively coupled plasma mass spectrometry (ICP-MS) with an Agilent 7500CE. High-resolution core-level and valence-band (VB) X-ray photoelectron spectroscopy (XPS) was conducted with a Kratos AXIS ULtrabld spectrometer equipped with monochromatic Al Kα radiation. The binding energies were measured with an accuracy of 0.1 eV, which were calibrated using the C 1s peak at 284.6 eV from carbon contamination. Fitting of the Pt 4f core-level XPS was performed using two spin−orbit split Pt $4f_{7/2}$ and $4f_{5/2}$ components, which are separated by 3.33 eV with a fixed area ratio of 4/3. The VB-XPS spectra of the Pt nanoparticles were obtained by subtracting the polymer contributions from the as-obtained VB-XPS profiles. The analyzer was in the constant analyzer energy (CAE) mode at a pass energy of 30 eV for all the VB-XPS measurements. The valence band maximum (VBM) was determined by extrapolating the excited leading edge to the energy axis as a reference of the d-band center.[39] The d-band center was located at the point which splits the VB-XPS spectrum into two parts of equal area.

3. RESULTS AND DISCUSSION

In this work, the synthesis of polymer nanoshells for stabilizing Pt nanoparticles relies on the formation of an ethanol/water emulsion induced by different solubility of SDBS in the respective solvents (Figure 1a). While SDBS is highly soluble in water by forming micelles, it is insoluble in a solvent of a lower polarity, ethanol for example. Therefore, when ethanol is introduced into the micellar solution of SDBS, phase separation can be induced, which results in an ethanol/water emulsion

DOI: 10.1021/acsami.6b16857
ACS Appl. Mater. Interfaces 2017, 9, 9710−9717

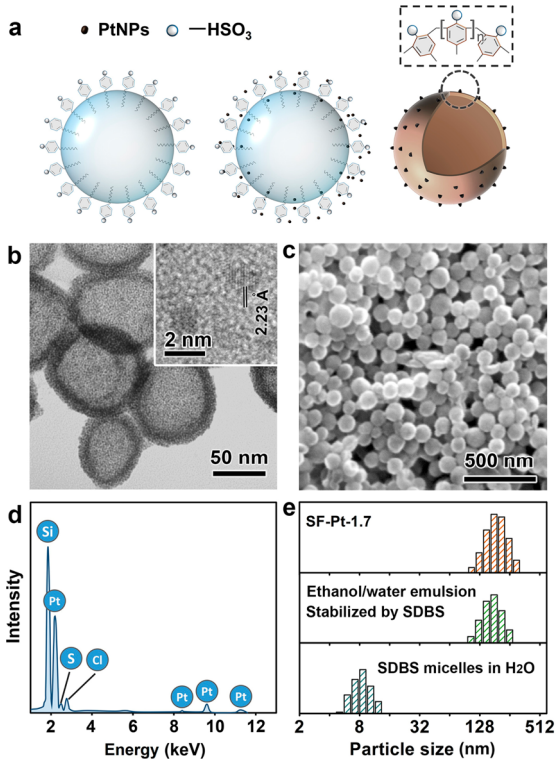

Figure 1. Synthesis of Pt nanoparticles immobilized on hollow SDBS-formaldehyde polymer nanospheres (SF-Pt-*x*, *x*: size of the Pt nanoparticles, unit: nm). (a) A scheme illustrating the formation mechanism of the hollow SF-Pt-*x* nanospheres. (b, c) TEM and SEM images of SF-Pt-1.7, respectively. Inset: HRTEM of a Pt nanoparticle showing (111) fringes. (d) EDS of SF-Pt-1.7. The signal of Si is from the silicon substrate. (e) In-situ DLS for monitoring the size of the colloids during the synthesis, including SDBS micelles formed in water, ethanol/water emulsion stabilized by SDBS, and the final hollow nanospheres after polymerization with formaldehyde.

with SDBS dissolving in the water phase and stabilizing the interface. The emulsification process can be conveniently monitored by DLS analysis, which shows a significant increase in the hydrodynamic size of the colloids from ~8 (micelles) to ~180 nm (emulsion) (Figure 1e). The size of the emulsions can be readily tuned from 144 to 523 nm by tuning the ethanol/water ratio upon dissolution of SDBS, as determined by the DLS, which can be further visualized by hollow nanospheres of a resin obtained by templating against these emulsions (Supporting Information Table S1 and Figures S1 and S2). The convenient tuning of size of the emulsions enables production of a rich class of polymer nanoshells as a support for noble metal nanoparticles.

The SDBS molecules assembled at the ethanol/water interface proved to be polymerizable due to the presence of the benzene rings, resembling the polymerization reactions in affording phenol-formaldehyde or resorcinol-formaldehyde (RF) resins.[40−42] Thus, polymeric hollow nanospheres were obtained by introducing formaldehyde into the emulsion system. On the other hand, with formaldehyde dually acting as the reducing agent, Pt nanoparticles can be formed in situ and stabilized on the SDBS-formaldehyde polymer nanoshells via the electrostatic interactions (Figure 1a). The abundant sulfonate groups on the polymer nanoshells provide excellent anchoring sites for the Pt nanoparticles. The TEM image of the resulting composites, denoted as SF-Pt-*x* (*x*, size of the Pt nanoparticles in nanometer), shows clear interior cavities and thus a hollow nanostructure (Figure 1b). The SEM image demonstrates uniform spherical morphology of the material and ~200 nm of the overall size (Figure 1c), which is consistent with the DLS measurement (Figure 1e), confirming that the nanoshells were obtained by polymerization of SDBS at the interface of the ethanol/water emulsions (Figure 1d). Pt nanoparticles of a high density can be found on the polymer nanoshells (Figure 1b). These Pt nanoparticles are highly uniform with an average size of ~1.7 nm, suggesting that Pt nanoparticles can be produced with uniform size and effectively stabilized by the polymer nanoshells by this method. HRTEM image of a single Pt nanoparticle shows clear fringes with spacing of ~2.23 Å, which correspond to the {100} planes of a Pt lattice (Figure 1b, inset). The elemental analysis by EDS confirms the presence of Pt, Cl, and S (Figure 1d), which can be attributed to the Pt nanoparticles, the remaining Cl^- from the platinum precursor (K_2PtCl_4), and the abundant sulfonate groups in the SDBS-formaldehyde polymer, respectively.

Therefore, synthesis and effective stabilization of ultrasmall Pt nanoparticles were successfully achieved in one pot by chemical reduction of a Pt precursor coupled with polymerization of SDBS at the interface of an ethanol/water emulsion. In addition, the size of the Pt nanoparticles can be precisely controlled by varying the concentration of the Pt precursor, K_2PtCl_4, in a typical synthesis, resulting in continuously growing Pt nanoparticles (0.9−2.3 nm) with increasing concentration of the Pt precursor. Figure 2a−d represents TEM images of the SF-Pt-*x* (*x* = 0.9, 1.4, 1.7, and 2.3) catalysts, which show ultrasmall Pt nanoparticles on the polymer nanoshells, all exhibiting uniform size distribution and absence of nanoparticle aggregates. The Pt nanoparticles are thus highly accessible on the shells, suitable for use as a catalyst for many

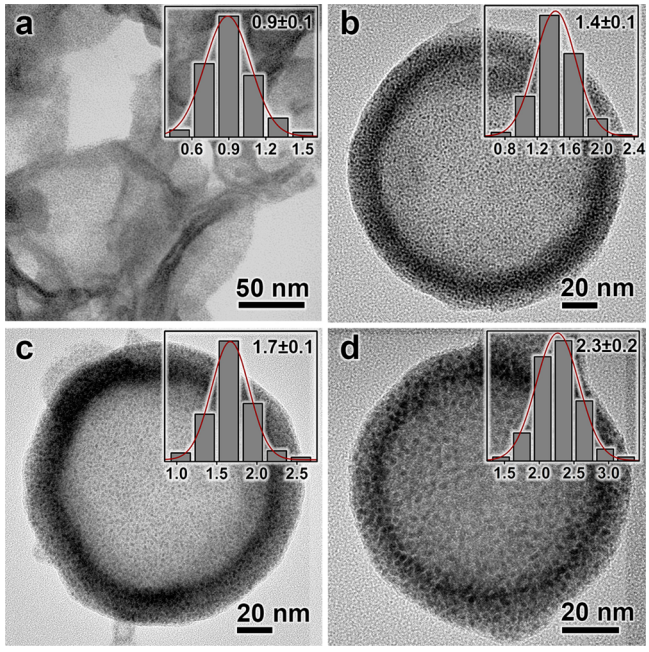

Figure 2. TEM images of the hollow SF-Pt-*x* nanospheres with Pt nanoparticles of varying sizes. (a−d) The sizes of the Pt nanoparticles (in terms of "mean value ± standard deviation") were 0.9 ± 0.1, 1.4 ± 0.1, 1.7 ± 0.1, and 2.3 ± 0.2 nm, respectively. Inset: Size distributions of the Pt nanoparticles measured from the HRTEM images (see Figures S6−S9); unit of the size: nm.

DOI: 10.1021/acsami.6b16857
ACS Appl. Mater. Interfaces 2017, 9, 9710−9717

organic reactions, especially those involving reactants of large molecules.

It should be noted that the size of Pt nanoparticles can also impose significant effect on the formation of the SDBS-formaldehyde polymer nanoshells. The polymer nanoshells decorated with Pt nanoparticles of 1.4, 1.7, and 2.3 nm are all spherical, while those decorated with Pt nanoparticles of 0.9 nm are irregular in shape (Figure 2, Figures S3 and S4). As revealed by TEM, the Pt nanoparticles are adsorbed at the interface of the emulsion, which are able to reduce the Helmholtz free energy and thus stabilize the emulsion architecture,[43] resembling a Pickering emulsion.[44] The decrease in the Helmholtz free energy depends on the size of the nanoparticles at the interface, with nanoparticles of large sizes facilitating reduction of the free energy. Thus, Pt nanoparticles of large sizes are able to retain the emulsion structures during the polymerization process (Figure 2b–d), while Pt nanoparticles of small sizes cannot stabilize the emulsion, leading to polymer with irregular shapes (Figure 2a). Under extreme conditions, when the polymerization was carried out in the absence of Pt nanoparticles, the emulsion templates collapsed and failed to afford hollow polymer nanoshells (Figure S2). The instability of the emulsions in the absence or presence of small Pt nanoparticles can be further confirmed by in situ DLS analysis, showing the presence of large polymer aggregates (Figure S5).

Crystal structures of the supported Pt nanoparticles were characterized by XRD (Figure 3a). The XRD pattern of SF-Pt-2.3 shows typical 111, 200, and 220 reflections from the Pt lattice. With a decrease in the size of the Pt nanoparticles, the respective reflection peaks undergo gradual broadening, and completely disappear when the size reaches 0.9 nm, suggesting a crystalline–amorphous transition of the Pt nanoparticles. The sizes of the Pt nanoparticles can be derived from the XRD pattern by the Scherrer equation, which are in high agreement with those calculated from the TEM observations (Figure 3b). The oxidation states of the Pt nanoparticles were analyzed by Pt 4f core-level XPS, which were then fitted by spin–orbit split $4f_{7/2}$ and $4f_{5/2}$ components (Figures 3c and S10). The fractions of Pt(0), Pt(II), and Pt(IV) can be therefore determined by measuring the areas of the respective peaks (Figure 3d). The Pt nanoparticles of 2.3, 1.7, and 1.4 nm are all composed of Pt(0) and Pt(II) species, with the Pt(II) species continuously increasing with decreasing particle size. When the size reaches 0.9 nm, the nanoparticles are composed of oxidative Pt(II) and Pt(IV) species. The oxygen in the high-valence Pt species might come from the ambient air. Thus, a metal–oxide transition has been observed with decreasing size of the Pt nanoparticles, which is coincident with previous observations.[33,45]

In our previous study, we found that the catalytic property of Pt nanoparticles on an inert resorcinol-formaldehyde resin can be correlated with their d-band electron structures,[33] which are proportional to the density of states, and directly related with the bonding strength of the Pt nanoparticles and the guest molecules.[46,47] To further evaluate this interaction, the d-band electron structures of the Pt nanoparticles on the polymer shells were characterized by high-resolution valence-band XPS (Figure 3e). The d-band center was determined with reference to the valence band maximum (VBM) (Figure 3f). A narrowing of the d electron bands can be observed with decreasing size of the Pt nanoparticles, which results in a significant upward shift of the d-band center and thus stronger interactions with a guest molecule. As this rule is general and applicable to guest molecules of a great variety, we expected that the SF-Pt-*x*

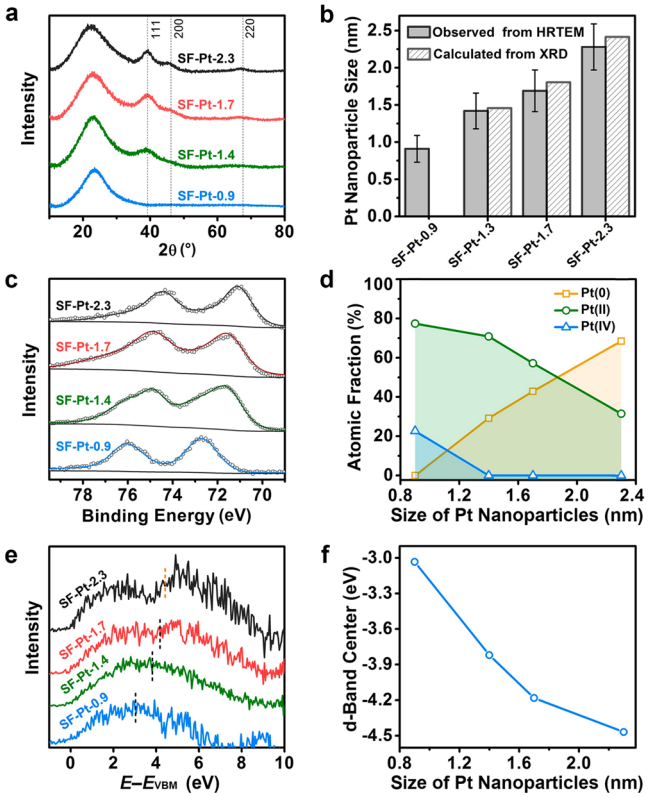

Figure 3. Structural, compositional, and electronic properties of the SF-Pt-*x* (*x* = 0.9, 1.4, 1.7, and 2.3). (a) XRD patterns of SF-Pt-*x*. (b) Comparison of the grain sizes calculated by the Scherrer equation from their XRD patterns with those observed from HRTEM. (c) Core-level Pt 4f XPS of the SF-Pt-*x*. (d) Oxidation state fractions of the Pt nanoparticles as a function of their size, derived from the core-level Pt 4f XPS. (e) High-resolution valence-band Pt 5d XPS of SF-Pt-*x* relative to the valence band maximum (VBM). Dashed lines indicate the d-band centers. (f) Plot of the d-band center (vs VBM) as a function of the size of the Pt nanoparticles.

catalysts exhibit size-dependent catalytic property in a spectrum of organic reactions.

The catalytic property of the SF-Pt-*x* catalysts were examined in a family of organic oxidation reactions, which was exemplified by aerobic oxidation of 1-phenylethanol (80 °C, 1 atm air) (Figure 4). Commercial Pt/C (size of Pt nanoparticles, 3.2 nm) was employed as a reference. Over commercial Pt/C and SF-Pt-2.3, the conversions of 1-phenylethanol reached only ~11% and ~1%, respectively, after 8 h of the reaction (Figure 4b). When the size of the Pt nanoparticles was decreased to 1.7 nm, the conversion reached ~100% in ~8 h, showing astonishingly high catalytic activity. The reaction rates over Pt nanoparticles of even smaller sizes, 1.4 and 0.9 nm, dropped significantly, with conversions of only ~13.3% and ~1% after 8 h of the reaction. It is therefore obvious that the size of the Pt nanoparticles imposes critical effect on their catalytic activity, with an appropriately small size showing optimal activity in oxidation of alcohol at 80 °C and ambient aerobic pressure. The selectivity toward the desired acetophenone was >99% according to the GC–MS analysis.

The turnover frequencies (TOFs) were calculated as a measure of the intrinsic catalytic activity of the Pt nanoparticles normalized by their surface Pt atoms, assuming that all Pt nanoparticles are accessible by the reactants (Figure 4c). With decreasing size of the Pt nanoparticles, the TOF values first

DOI: 10.1021/acsami.6b16857
ACS Appl. Mater. Interfaces 2017, 9, 9710–9717

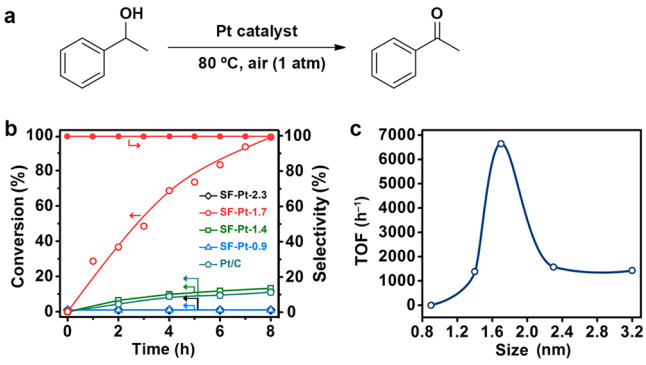

Figure 4. Catalytic activities of the SF-Pt-*x* catalysts (*x* = 0.9, 1.4, 1.7, and 2.3) in aerobic oxidation of 1-phenylethanol. (a) Products of the 1-phenylethanol oxidation reaction. (b) Plot of conversion of 1-phenylethanol versus reaction time. The reaction was conducted in water open to air (1 atm) at 80 °C, with catalysts of 2 mol % of the substrate. No extra solvent was used in the catalysis. (c) Plot of TOF against the size of the Pt nanoparticles. The reaction was carried out in air (1 atm) at 120 °C, with catalyst of 0.028 mol‰ of the substrate.

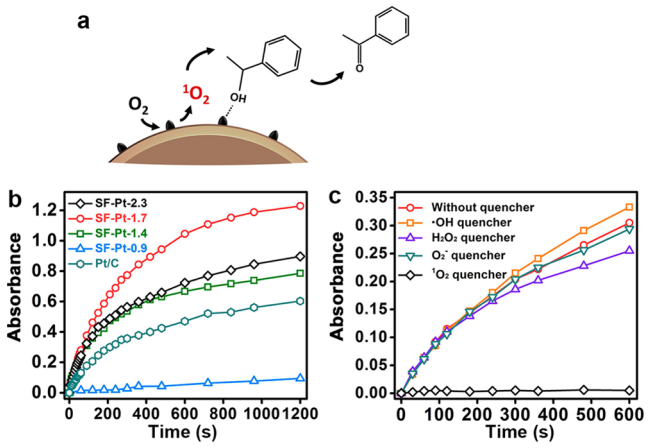

Figure 5. (a) Possible pathway of the oxidation of 1-phenylethanol. (b) Plot of absorbance of TMB oxidation products at 652 nm versus reaction time by employing SF-Pt-*x* (*x* = 0.9, 1.4, 1.7, and 2.3) and Pt/C as the catalysts. (c) Plot of absorbance of TMB oxidation products at 652 nm in the presence of various scavenger molecules.

increase and then decrease, reaching a maximum when the size of the Pt nanoparticles was 1.7 nm. Thus, a volcano-shape profile of the activity versus particle size can be observed. It is worth noting that the TOF value of SF-Pt-1.7 reached a remarkable 7000 h^{-1}, which is among the highest values that have been achieved by far in Pt-catalyzed oxidation of 1-phenylethanol, although the reaction conditions are not perfectly the same (Table S3).[48−52] Therefore, it can be concluded that Pt nanoparticles exhibit strong size effect in organic oxidation reactions. Conventionally, catalysts for organic oxidation reactions include Pd nanoparticles,[53] semiconductors,[54−56] and carbon materials,[57] and so forth. In this work, we have optimized the activity of Pt nanoparticles for this important family of organic reactions by facilely tuning their size (Table S2). It is worth noting that supports, N-doped carbon for example, usually provide strong metal−support interactions with metal nanoparticles, which not only help to stabilize noble metal nanoparticles, but also significantly modify their catalytic activity due to the effect of electron transfer.[53,58−62] In this work, we employed sulfonates in the SF polymer to anchor the Pt nanoparticles. Although there is a similar stabilization effect, no clear effect of the support has been observed on the catalytic activity of the Pt nanoparticles (Figure S15), which suggests that the volcano-shaped profile of TOF as a function of the particle size reflects the intrinsic catalytic property of the Pt nanoparticles.

To further understand the size-dependent catalytic property of Pt nanoparticles in organic oxidation reactions, activation of oxygen on these catalysts was investigated (Figure 5). In a typical experiment, 3,5,3′,5′-tetramethylbenzidine (TMB) was introduced into the buffer solution in the presence of the SF-Pt-*x* catalysts under ambient aerobic conditions. TMB can be readily oxidized by activated oxygen species to afford two chromophoric products via a one-electron oxidation process, which show absorption bands at 370 and 652 nm, and therefore can be easily detected by routine UV−vis spectroscopy (Figures S12 and S13).[63] Immediately after mixing the TMB with the catalysts, the absorbance at 652 nm started to increase, indicating the activation of oxygen by the Pt nanoparticles (Figure 5b). SF-Pt-1.7 exhibited the highest kinetics of the oxygen activation, compared with catalysts with either smaller or larger Pt nanoparticles. Therefore, the size of the Pt nanoparticles imposes strong effect on the oxygen activation reaction. The interaction between oxygen and Pt nanoparticles of ∼1.7 nm is neither too strong nor too weak for favorable activation kinetics. To further clarify the activated oxygen species by the Pt nanoparticles, different scavengers were introduced into the reaction system, including carotene, mannite, catalase, and SOD that are typical scavengers for $^1O_2$, •OH, H_2O_2, and O_2^-, respectively (Figures 5c and S14).[64] Obviously, only carotene can effectively prohibit the oxidation of TMB, confirming that the oxygen was activated into singlet oxygen $^1O_2$ by the Pt nanoparticles, which is a result of the electron donation from Pt 5d to the antibonding $2\pi^*$ orbital of O_2.

When comparing Figure 5b with Figure 4b, it can be concluded that the size effect is much stronger in the overall 1-phenylethanol oxidation reaction than that in the oxygen activation reaction, which suggests that the rate-determining step is the oxidation of 1-phenylethanol, while the oxygen activation step occurs in a much favorable rate. Therefore, the interaction between Pt nanoparticles and 1-phenylethanol plays a very critical role in determining the overall reaction rate. Similar to the interaction between Pt nanoparticles and oxygen, as described above, it is reasonable that Pt nanoparticles of decreasing sizes possess increasing interaction with 1-phenylethanol, according to the analysis of the d-band electron structure of the Pt nanoparticles, which leads to an accelerated rate of the oxidation reaction between 1-phenylethanol and the activated $^1O_2$ species. However, when the size of the Pt nanoparticles was too small (1.4 and 0.9 nm), the interactions between the reactants and the catalyst were too strong for their convenient departure from the catalysts, leading to poisoning of the catalyst and thus significantly decreased kinetics of the overall oxidation reaction. By this means, the size-dependent catalytic activity of Pt nanoparticles in aerobic oxidation reaction of 1-phenylethanol can be rationalized.

On the basis of the above analysis, a reaction pathway of Pt-catalyzed 1-phenylethanol oxidation reaction can be proposed as follows (Figure 5a). Initially, oxygen was chemisorbed on the surface of the Pt nanoparticles and dissociated into singlet $^1O_2$ species. At the same time, 1-phenylethanol was chemisorbed on

DOI: 10.1021/acsami.6b16857
ACS Appl. Mater. Interfaces 2017, 9, 9710−9717

the Pt nanoparticles and dissociated to form Pt-alkoxide species, as suggested by previous experiments and DFT calculations.[65,66] Then, the 1-phenylethanol molecules were oxidized by the adjacent $^1O_2$ species, followed by leaving of the product (acetophenone) from the surface of the Pt nanoparticles. The rate of the oxidation reaction depends on the interactions between the Pt nanoparticles and the reactants/products, which can be readily tuned by the size of the Pt nanoparticles.

It is interesting to note that our previous work demonstrated strong size effect of the Pt nanoparticles on their catalytic activity in hydrogenation of quinoline.[33] Similar to the oxidation reaction of 1-phenylethanol as demonstrated in this work, a volcano-shape profile of the TOF as a function of the particle size was also observed, confirming the generality of the size effect of noble metal nanoparticles in different reaction systems. Among different sizes, Pt nanoparticles of 1.2 nm showed the highest activity in hydrogenation of quinoline, which is different from the optimal size of Pt nanoparticles (1.7 nm) for the oxidation reaction of 1-phenylethanol. The difference in the optimal size may arise from the different bond strengths of quinoline and 1-phenylethanol with the Pt nanoparticles. The optimal size of the Pt nanoparticles thus varies to achieve their respective bond strength that is appropriate for the reactions.

The SF polymer nanoshells as a support for the Pt nanoparticle are stable at low reaction temperatures, which are prone to oxidation at a high temperature, leading to aggregation of the ultrasmall Pt nanoparticles, and thus significant deactivation of the catalyst (Figure S16). We propose that carbonization of the polymer shells while retaining the ultrasmall size of the Pt nanoparticles may potentially help to maintain the high catalytic activity of the catalysts with a much improved durability under many harsh conditions, which is under investigation and will be presented in a future report.

4. CONCLUSIONS

In summary, we have presented a novel strategy to synthesize and stabilize uniform Pt nanoparticles with ultrasmall sizes on SDBS-formaldehyde polymer nanoshells. For the first time, the SDBS molecules can be polymerized with formaldehyde at the interface of an ethanol/water emulsion, forming discrete polymer nanoshells. The size of the nanoshells can be conveniently tuned in a range of 144 to 523 nm. The abundant sulfonate groups render the nanoshells with high affinity to Pt nanoparticles, making them excellent supports for the Pt nanoparticles. The resulting catalyst showed strong size effect in catalyzing a family of organic oxidation reactions, which has been exemplified by aerobic oxidation of 1-phenylethanol to yield acetophenone. Pt nanoparticles of ~1.7 nm showed the highest catalytic activity in this reaction, with the turnover frequency reaching 7000 h^{-1}, which is among the highest values that have been achieved by far with Pt catalysts for this reaction. The size effect has been rationalized by the size-dependent d-band electron structure of the Pt nanoparticles. This work confirms that the size effect of Pt nanoparticles is not restricted to the organic hydrogenation reactions, as demonstrated in our previous work, but is also applicable in general organic oxidation reactions, thus providing general methodology for the design of metal-nanoparticle-based catalysts for fine-chemical production with high activity.

ASSOCIATED CONTENT

Supporting Information

The Supporting Information is available free of charge on the ACS Publications website at DOI: 10.1021/acsami.6b16857.

Size tuning of the ethanol/water emulsion stabilized by SDBS, HRTEM images and XPS spectra of the SF-Pt-*x*, additional results and discussion on the synthesis of the SF-Pt-*x* and their catalytic mechanism, deactivation of the catalyst, extension of the catalytic system to oxidation of other substrates, and comparison of the results with those from literature (PDF)

AUTHOR INFORMATION

Corresponding Authors

*E-mail: gaochuanbo@mail.xjtu.edu.cn (C.G.).
*E-mail: chenqiang2204@mail.xjtu.edu.cn (Q.C.).

ORCID

Chuanbo Gao: 0000-0003-3429-3473

Author Contributions

The manuscript was written through contributions of all authors. All authors have given approval to the final version of the manuscript.

Notes

The authors declare no competing financial interest.

ACKNOWLEDGMENTS

C.G. acknowledges support from the National Natural Science Foundation of China (21671156, 21301138). Q.C. acknowledges support from the China Postdoctoral Science Foundation (2015M582634) and the Fundamental Research Funds for the Central Universities provided by Xi'an Jiaotong University (xjj2015033).

REFERENCES

(1) Astruc, D.; Lu, F.; Aranzaes, J. R. Nanoparticles as Recyclable Catalysts: The Frontier between Homogeneous and Heterogeneous Catalysis. *Angew. Chem., Int. Ed.* **2005**, *44*, 7852−7872.

(2) Hashmi, A. S.; Hutchings, G. J. Gold Catalysis. *Angew. Chem., Int. Ed.* **2006**, *45*, 7896−7936.

(3) *Metal Nanoparticles for Catalysis: Advances and Applications*; Tao, F., Ed.; Royal Society of Chemistry: Cambridge, U.K., 2014.

(4) Haruta, M.; Kobayashi, T.; Sano, H.; Yamada, N. Novel Gold Catalysts for the Oxidation of Carbon Monoxide at a Temperature Far Below 0 °C. *Chem. Lett.* **1987**, *16*, 405−408.

(5) Valden, M.; Lai, X.; Goodman, D. W. Onset of Catalytic Activity of Gold Clusters on Titania with the Appearance of Nonmetallic Properties. *Science* **1998**, *281*, 1647−1650.

(6) Ding, K.; Gulec, A.; Johnson, A. M.; Schweitzer, N. M.; Stucky, G. D.; Marks, L. D.; Stair, P. C. Identification of Active Sites in Co Oxidation and Water-Gas Shift over Supported Pt Catalysts. *Science* **2015**, *350*, 189−192.

(7) Yamamoto, K.; Imaoka, T.; Chun, W. J.; Enoki, O.; Katoh, H.; Takenaga, M.; Sonoi, A. Size-Specific Catalytic Activity of Platinum Clusters Enhances Oxygen Reduction Reactions. *Nat. Chem.* **2009**, *1*, 397−402.

(8) Toyoda, E.; Jinnouchi, R.; Hatanaka, T.; Morimoto, Y.; Mitsuhara, K.; Visikovskiy, A.; Kido, Y. The D-Band Structure of Pt Nanoclusters Correlated with the Catalytic Activity for an Oxygen Reduction Reaction. *J. Phys. Chem. C* **2011**, *115*, 21236−21240.

(9) Perez-Alonso, F. J.; McCarthy, D. N.; Nierhoff, A.; Hernandez-Fernandez, P.; Strebel, C.; Stephens, I. E.; Nielsen, J. H.; Chorkendorff, I. The Effect of Size on the Oxygen Electroreduction Activity of Mass-Selected Platinum Nanoparticles. *Angew. Chem., Int. Ed.* **2012**, *51*, 4641−4643.

DOI: 10.1021/acsami.6b16857
ACS Appl. Mater. Interfaces 2017, 9, 9710−9717

(10) Imaoka, T.; Kitazawa, H.; Chun, W. J.; Omura, S.; Albrecht, K.; Yamamoto, K. Magic Number Pt13 and Misshapen Pt12 Clusters: Which One Is the Better Catalyst? *J. Am. Chem. Soc.* **2013**, *135*, 13089−13095.
(11) Imaoka, T.; Kitazawa, H.; Chun, W. J.; Yamamoto, K. Finding the Most Catalytically Active Platinum Clusters with Low Atomicity. *Angew. Chem., Int. Ed.* **2015**, *54*, 9810−9815.
(12) Huang, L.; Han, B.; Xi, Y.; Forrey, R. C.; Cheng, H. Influence of Charge on the Reactivity of Supported Heterogeneous Transition Metal Catalysts. *ACS Catal.* **2015**, *5*, 4592−4597.
(13) Wang, H.; Wang, Y.; Zhu, Z.; Sapi, A.; An, K.; Kennedy, G.; Michalak, W. D.; Somorjai, G. A. Influence of Size-Induced Oxidation State of Platinum Nanoparticles on Selectivity and Activity in Catalytic Methanol Oxidation in the Gas Phase. *Nano Lett.* **2013**, *13*, 2976−2979.
(14) Corma, A.; Concepcion, P.; Boronat, M.; Sabater, M. J.; Navas, J.; Yacaman, M. J.; Larios, E.; Posadas, A.; Lopez-Quintela, M. A.; Buceta, D.; Mendoza, E.; Guilera, G.; Mayoral, A. Exceptional Oxidation Activity with Size-Controlled Supported Gold Clusters of Low Atomicity. *Nat. Chem.* **2013**, *5*, 775−781.
(15) Wei, H.; Liu, X.; Wang, A.; Zhang, L.; Qiao, B.; Yang, X.; Huang, Y.; Miao, S.; Liu, J.; Zhang, T. Feox-Supported Platinum Single-Atom and Pseudo-Single-Atom Catalysts for Chemoselective Hydrogenation of Functionalized Nitroarenes. *Nat. Commun.* **2014**, *5*, 5634.
(16) Huang, W.; Kuhn, J. N.; Tsung, C.-K.; Zhang, Y.; Habas, S. E.; Yang, P.; Somorjai, G. A. Dendrimer Templated Synthesis of One Nanometer Rh and Pt Particles Supported on Mesoporous Silica: Catalytic Activity for Ethylene and Pyrrole Hydrogenation. *Nano Lett.* **2008**, *8*, 2027−2034.
(17) Zhang, H.; Jin, M.; Xiong, Y.; Lim, B.; Xia, Y. Shape-Controlled Synthesis of Pd Nanocrystals and Their Catalytic Applications. *Acc. Chem. Res.* **2013**, *46*, 1783−1794.
(18) Solla-Gullon, J.; Vidal-Iglesias, F. J.; Feliu, J. M. Shape Dependent Electrocatalysis. *Annu. Rep. Prog. Chem., Sect. C: Phys. Chem.* **2011**, *107*, 263−297.
(19) Lim, B.; Jiang, M.; Camargo, P. H. C.; Cho, E. C.; Tao, J.; Lu, X.; Zhu, Y.; Xia, Y. Pd-Pt Bimetallic Nanodendrites with High Activity for Oxygen Reduction. *Science* **2009**, *324*, 1302−1305.
(20) Tian, N.; Zhou, Z. Y.; Sun, S. G.; Ding, Y.; Wang, Z. L. Synthesis of Tetrahexahedral Platinum Nanocrystals with High-Index Facets and High Electro-Oxidation Activity. *Science* **2007**, *316*, 732−735.
(21) Zhang, L.; Roling, L. T.; Wang, X.; Vara, M.; Chi, M.; Liu, J.; Choi, S.-I.; Park, J.; Herron, J. A.; Xie, Z.; Mavrikakis, M.; Xia, Y. Platinum-Based Nanocages with Subnanometer-Thick Walls and Well-Defined, Controllable Facets. *Science* **2015**, *349*, 412−416.
(22) Chiu, C.-Y.; Chung, P.-J.; Lao, K.-U.; Liao, C.-W.; Huang, M. H. Facet-Dependent Catalytic Activity of Gold Nanocubes, Octahedra, and Rhombic Dodecahedra toward 4-Nitroaniline Reduction. *J. Phys. Chem. C* **2012**, *116*, 23757−23763.
(23) Wang, G. H.; Hilgert, J.; Richter, F. H.; Wang, F.; Bongard, H. J.; Spliethoff, B.; Weidenthaler, C.; Schuth, F. Platinum-Cobalt Bimetallic Nanoparticles in Hollow Carbon Nanospheres for Hydrogenolysis of 5-Hydroxymethylfurfural. *Nat. Mater.* **2014**, *13*, 293−300.
(24) Tedsree, K.; Li, T.; Jones, S.; Chan, C. W.; Yu, K. M.; Bagot, P. A.; Marquis, E. A.; Smith, G. D.; Tsang, S. C. Hydrogen Production from Formic Acid Decomposition at Room Temperature Using a Ag-Pd Core-Shell Nanocatalyst. *Nat. Nanotechnol.* **2011**, *6*, 302−307.
(25) Stamenkovic, V. R.; Mun, B. S.; Arenz, M.; Mayrhofer, K. J. J.; Lucas, C. A.; Wang, G.; Ross, P. N.; Markovic, N. M. Trends in Electrocatalysis on Extended and Nanoscale Pt-Bimetallic Alloy Surfaces. *Nat. Mater.* **2007**, *6*, 241−247.
(26) Che, M.; Bennett, C. O. The Influence of Particle Size on the Catalytic Properties of Supported Metals. In *Advances in Catalysis*; Eley, H. P.; Paul, B. W., Eds.; Academic Press: New York,1989; Vol. *36*, pp 55−172.
(27) Zhu, Y.; Zaera, F. Selectivity in the Catalytic Hydrogenation of Cinnamaldehyde Promoted by Pt/Sio2as a Function of Metal Nanoparticle Size. *Catal. Sci. Technol.* **2014**, *4*, 955−962.
(28) Prashar, A. K.; Mayadevi, S.; Nandini Devi, R. Effect of Particle Size on Selective Hydrogenation of Cinnamaldehyde by Pt Encapsulated in Mesoporous Silica. *Catal. Commun.* **2012**, *28*, 42−46.
(29) Dhiman, M.; Polshettiwar, V. Ultrasmall Nanoparticles and Pseudo-Single Atoms of Platinum Supported on Fibrous Nanosilica (Kcc-1/Pt): Engineering Selectivity of Hydrogenation Reactions. *J. Mater. Chem. A* **2016**, *4*, 12416−12424.
(30) Kuhn, J. N.; Huang, W.; Tsung, C.-K.; Zhang, Y.; Somorjai, G. A. Structure Sensitivity of Carbon−Nitrogen Ring Opening: Impact of Platinum Particle Size from Below 1 to 5 Nm Upon Pyrrole Hydrogenation Product Selectivity over Monodisperse Platinum Nanoparticles Loaded onto Mesoporous Silica. *J. Am. Chem. Soc.* **2008**, *130*, 14026−14027.
(31) Tsung, C.-K.; Kuhn, J. N.; Huang, W.; Aliaga, C.; Hung, L.-I.; Somorjai, G. A.; Yang, P. Sub-10 Nm Platinum Nanocrystals with Size and Shape Control: Catalytic Study for Ethylene and Pyrrole Hydrogenation. *J. Am. Chem. Soc.* **2009**, *131*, 5816−5822.
(32) Pushkarev, V. V.; Musselwhite, N.; An, K.; Alayoglu, S.; Somorjai, G. A. High Structure Sensitivity of Vapor-Phase Furfural Decarbonylation/Hydrogenation Reaction Network as a Function of Size and Shape of Pt Nanoparticles. *Nano Lett.* **2012**, *12*, 5196−5201.
(33) Bai, L.; Wang, X.; Chen, Q.; Ye, Y.; Zheng, H.; Guo, J.; Yin, Y.; Gao, C. Explaining the Size Dependence in Platinum-Nanoparticle-Catalyzed Hydrogenation Reactions. *Angew. Chem., Int. Ed.* **2016**, *55*, 15656−15661.
(34) Zhang, T.; Zhao, H.; He, S.; Liu, K.; Liu, H.; Yin, Y.; Gao, C. Unconventional Route to Encapsulated Ultrasmall Gold Nanoparticles for High-Temperature Catalysis. *ACS Nano* **2014**, *8*, 7297−7304.
(35) Zhao, H.; Wang, D.; Gao, C.; Liu, H.; Han, L.; Yin, Y. Ultrafine Platinum/Iron Oxide Nanoconjugates Confined in Silica Nanoshells for Highly Durable Catalytic Oxidation. *J. Mater. Chem. A* **2016**, *4*, 1366−1372.
(36) Rioux, R. M.; Song, H.; Hoefelmeyer, J. D.; Yang, P.; Somorjai, G. A. High-Surface-Area Catalyst Design: Synthesis, Characterization, and Reaction Studies of Platinum Nanoparticles in Mesoporous Sba-15 Silica. *J. Phys. Chem. B* **2005**, *109*, 2192−2202.
(37) Xiao, C.; Maligal-Ganesh, R. V.; Li, T.; Qi, Z.; Guo, Z.; Brashler, K. T.; Goes, S.; Li, X.; Goh, T. W.; Winans, R. E.; Huang, W. High-Temperature-Stable and Regenerable Catalysts: Platinum Nanoparticles in Aligned Mesoporous Silica Wells. *ChemSusChem* **2013**, *6*, 1915−1922.
(38) Herzing, A. A.; Kiely, C. J.; Carley, A. F.; Landon, P.; Hutchings, G. J. Identification of Active Gold Nanoclusters on Iron Oxide Supports for Co Oxidation. *Science* **2008**, *321*, 1331−1335.
(39) Chambers, S. A.; Droubay, T.; Kaspar, T. C.; Gutowski, M.; van Schilfgaarde, M. Accurate Valence Band Maximum Determination for Srtio3(0 0 1). *Surf. Sci.* **2004**, *554*, 81−89.
(40) Meng, Y.; Gu, D.; Zhang, F.; Shi, Y.; Yang, H.; Li, Z.; Yu, C.; Tu, B.; Zhao, D. Ordered Mesoporous Polymers and Homologous Carbon Frameworks: Amphiphilic Surfactant Templating and Direct Transformation. *Angew. Chem., Int. Ed.* **2005**, *44*, 7053−7059.
(41) Liu, J.; Qiao, S. Z.; Liu, H.; Chen, J.; Orpe, A.; Zhao, D.; Lu, G. Q. Extension of the Stober Method to the Preparation of Monodisperse Resorcinol-Formaldehyde Resin Polymer and Carbon Spheres. *Angew. Chem., Int. Ed.* **2011**, *50*, 5947−5951.
(42) Li, N.; Zhang, Q.; Liu, J.; Joo, J.; Lee, A.; Gan, Y.; Yin, Y. Sol-Gel Coating of Inorganic Nanostructures with Resorcinol-Formaldehyde Resin. *Chem. Commun.* **2013**, *49*, 5135−5137.
(43) Lin, Y.; Skaff, H.; Emrick, T.; Dinsmore, A. D.; Russell, T. P. Nanoparticle Assembly and Transport at Liquid-Liquid Interfaces. *Science* **2003**, *299*, 226−229.
(44) Pickering, S. U. Cxcvi.-Emulsions. *J. Chem. Soc., Trans.* **1907**, *91*, 2001−2021.
(45) Wang, H.; Wang, Y.; Zhu, Z.; Sapi, A.; An, K.; Kennedy, G.; Michalak, W. D.; Somorjai, G. A. Influence of Size-Induced Oxidation State of Platinum Nanoparticles on Selectivity and Activity in Catalytic Methanol Oxidation in the Gas Phase. *Nano Lett.* **2013**, *13*, 2976−2979.

DOI: 10.1021/acsami.6b16857
ACS Appl. Mater. Interfaces 2017, 9, 9710−9717

(46) King, P. D. C.; Veal, T. D.; Schleife, A.; Zúñiga-Pérez, J.; Martel, B.; Jefferson, P. H.; Fuchs, F.; Muñoz-Sanjosé, V.; Bechstedt, F.; McConville, C. F. Valence-Band Electronic Structure of Cdo, Zno, and Mgo from X-Ray Photoemission Spectroscopy and Quasi-Particle-Corrected Density-Functional Theory Calculations. *Phys. Rev. B: Condens. Matter Mater. Phys.* **2009**, *79*, 205205.
(47) Hammer, B.; Norskov, J. K. Why Gold Is the Noblest of All the Metals. *Nature* **1995**, *376*, 238−240.
(48) Hong, H.; Hu, L.; Li, M.; Zheng, J.; Sun, X.; Lu, X.; Cao, X.; Lu, J.; Gu, H. Preparation of Pt@Fe2o3 Nanowires and Their Catalysis of Selective Oxidation of Olefins and Alcohols. *Chem. - Eur. J.* **2011**, *17*, 8726−8730.
(49) Karimi, B.; Naderi, Z.; Khorasani, M.; Mirzaei, H. M.; Vali, H. Ultrasmall Platinum Nanoparticles Supported inside the Nanospaces of Periodic Mesoporous Organosilica with an Imidazolium Network: An Efficient Catalyst for the Aerobic Oxidation of Unactivated Alcohols in Water. *ChemCatChem* **2016**, *8*, 906−910.
(50) Ng, Y. H.; Ikeda, S.; Harada, T.; Morita, Y.; Matsumura, M. An Efficient and Reusable Carbon-Supported Platinum Catalyst for Aerobic Oxidation of Alcohols in Water. *Chem. Commun.* **2008**, 3181−3183.
(51) Shiraishi, Y.; Tsukamoto, D.; Sugano, Y.; Shiro, A.; Ichikawa, S.; Tanaka, S.; Hirai, T. Platinum Nanoparticles Supported on Anatase Titanium Dioxide as Highly Active Catalysts for Aerobic Oxidation under Visible Light Irradiation. *ACS Catal.* **2012**, *2*, 1984−1992.
(52) Yamada, Y. M. A.; Arakawa, T.; Hocke, H.; Uozumi, Y. A Nanoplatinum Catalyst for Aerobic Oxidation of Alcohols in Water. *Angew. Chem., Int. Ed.* **2007**, *46*, 704−706.
(53) Zhang, P.; Gong, Y.; Li, H.; Chen, Z.; Wang, Y. Solvent-Free Aerobic Oxidation of Hydrocarbons and Alcohols with Pd@N-Doped Carbon from Glucose. *Nat. Commun.* **2013**, *4*, 1593.
(54) Jia, H.; Zhu, X. M.; Jiang, R.; Wang, J. Aerosol-Sprayed Gold/Ceria Photocatalyst with Superior Plasmonic Hot Electron-Enabled Visible-Light Activity. *ACS Appl. Mater. Interfaces* **2017**, *9*, 2560−2571.
(55) Qamar, M.; Elsayed, R. B.; Alhooshani, K. R.; Ahmed, M. I.; Bahnemann, D. W. Highly Efficient and Selective Oxidation of Aromatic Alcohols Photocatalyzed by Nanoporous Hierarchical Pt/Bi2WO6 in Organic Solvent-Free Environment. *ACS Appl. Mater. Interfaces* **2015**, *7*, 1257−1269.
(56) Liu, L.; Ouyang, S.; Ye, J. Gold-Nanorod-Photosensitized Titanium Dioxide with Wide-Range Visible-Light Harvesting Based on Localized Surface Plasmon Resonance. *Angew. Chem., Int. Ed.* **2013**, *52*, 6689−6693.
(57) Yu, H.; Peng, F.; Tan, J.; Hu, X.; Wang, H.; Yang, J.; Zheng, W. Selective Catalysis of the Aerobic Oxidation of Cyclohexane in the Liquid Phase by Carbon Nanotubes. *Angew. Chem., Int. Ed.* **2011**, *50*, 3978−3982.
(58) Chen, X.; Wu, G.; Chen, J.; Chen, X.; Xie, Z.; Wang, X. Synthesis of "Clean" and Well-Dispersive Pd Nanoparticles with Excellent Electrocatalytic Property on Graphene Oxide. *J. Am. Chem. Soc.* **2011**, *133*, 3693−3695.
(59) Zhang, H.; Chen, S.; Quan, X.; Yu, H.; Zhao, H. In Situ Controllable Growth of Noble Metal Nanodot on Graphene Sheet. *J. Mater. Chem.* **2011**, *21*, 12986−12990.
(60) Shen, Y.; Zhang, Z.; Long, R.; Xiao, K.; Xi, J. Synthesis of Ultrafine Pt Nanoparticles Stabilized by Pristine Graphene Nanosheets for Electro-Oxidation of Methanol. *ACS Appl. Mater. Interfaces* **2014**, *6*, 15162−15170.
(61) He, L.; Weniger, F.; Neumann, H.; Beller, M. Synthesis, Characterization, and Application of Metal Nanoparticles Supported on Nitrogen-Doped Carbon: Catalysis Beyond Electrochemistry. *Angew. Chem., Int. Ed.* **2016**, *55*, 12582−12594.
(62) Perini, L.; Durante, C.; Favaro, M.; Perazzolo, V.; Agnoli, S.; Schneider, O.; Granozzi, G.; Gennaro, A. Metal-Support Interaction in Platinum and Palladium Nanoparticles Loaded on Nitrogen-Doped Mesoporous Carbon for Oxygen Reduction Reaction. *ACS Appl. Mater. Interfaces* **2015**, *7*, 1170−1179.
(63) Josephy, P. D.; Eling, T.; Mason, R. P. The Horseradish Peroxidase-Catalyzed Oxidation of 3,5,3′,5′-Tetramethylbenzidine. Free Radical and Charge-Transfer Complex Intermediates. *J. Biol. Chem.* **1982**, *257*, 3669−3675.
(64) Long, R.; Mao, K.; Ye, X.; Yan, W.; Huang, Y.; Wang, J.; Fu, Y.; Wang, X.; Wu, X.; Xie, Y.; Xiong, Y. Surface Facet of Palladium Nanocrystals: A Key Parameter to the Activation of Molecular Oxygen for Organic Catalysis and Cancer Treatment. *J. Am. Chem. Soc.* **2013**, *135*, 3200−3207.
(65) Dell'Anna, M. M.; Mali, M.; Mastrorilli, P.; Cotugno, P.; Monopoli, A. Oxidation of Benzyl Alcohols to Aldehydes and Ketones under Air in Water Using a Polymer Supported Palladium Catalyst. *J. Mol. Catal. A: Chem.* **2014**, *386*, 114−119.
(66) Mori, K.; Hara, T.; Mizugaki, T.; Ebitani, K.; Kaneda, K. Hydroxyapatite-Supported Palladium Nanoclusters: A Highly Active Heterogeneous Catalyst for Selective Oxidation of Alcohols by Use of Molecular Oxygen. *J. Am. Chem. Soc.* **2004**, *126*, 10657−10666.

DOI: 10.1021/acsami.6b16857
ACS Appl. Mater. Interfaces 2017, 9, 9710−9717